Letter

Scarring in classical chaotic dynamics with noise

Domenico Lippolis,[1] Akira Shudo,[2] Kensuke Yoshida,[2] and Hajime Yoshino[2]
[1]*Institute for Applied Systems Analysis, Jiangsu University, Zhenjiang 212013, China*
[2]*Department of Physics, Tokyo Metropolitan University, Minami-Osawa, Hachioji 192-0397, Japan*

(Received 23 January 2021; accepted 22 April 2021; published 7 May 2021)

We report the numerical observation of scarring, which is enhancement of probability density around unstable periodic orbits of a chaotic system, in the eigenfunctions of the classical Perron-Frobenius operator of noisy Anosov ("perturbed cat") maps, as well as in the noisy Bunimovich stadium. A parallel is drawn between classical and quantum scars, based on the unitarity or nonunitarity of the respective propagators. For uniformly hyperbolic systems such as the cat map, we provide a mechanistic explanation for the classical phase-space localization detected, based on the distribution of finite-time Lyapunov exponents, and the interplay of noise with deterministic dynamics. Classical scarring can be measured by studying autocorrelation functions and their power spectra.

DOI: 10.1103/PhysRevE.103.L050202

Introduction. In the realm of classical- and quantum chaos, phase-space densities tend to mix, due to the stretching and folding action of the dynamics. As a result, every form of localization is an anomaly to the expected "random" behavior of Hamiltonians, propagators, wave functions, and various observables.

Examples in quantum mechanics include dynamical localization for a kicked rotor [1], which can be related to the Anderson localization of a tight-binding model [2], opening-induced phase-space localization [3], and probability-density enhancement around unstable periodic orbits of the underlying classical system. The latter is known as scarring [4], and it has drawn a fair amount of attention since its first discovery in the quantum Bunimovich stadium billiard. Scars, the regions of enhanced probability density, have been ascribed to constructive interference around periodic orbits [5]. Dismissed for a while as transients of no effect on the long-term properties of a closed chaotic system subject to thermalization [6], scars were brought back into the spotlight by recent numerical evidence of ergodicity breaking in many-body systems [7–12]. Further theoretical and experimental work has extended the notion of scarring to regular dynamics [13–15], to integrable systems with disorder [16–18], of interest in cold atoms and condensed matter, as well as to relativistic Dirac billiards [19,20].

In the present paper, we report scarring in the eigenfunctions of the *classical* Perron-Frobenius evolution operator [21] with background noise, for two paradigmatic models of chaos. The observations presented here suggest that quantum localization in chaos does not exclusively arise from interference, but is also a classical effect.

The noiseless Perron-Frobenius operator

$$\mathcal{L}^t \rho(\mathbf{x}) = \int dx_0\, \delta(\mathbf{x} - f^t(\mathbf{x}_0))\rho(\mathbf{x}_0), \tag{1}$$

transports an initial phase-space density of trajectories $\rho(\mathbf{x})$ through the flow $f^t(\mathbf{x})$, that is the solution of the equations of motion, to a new density. The Perron-Frobenius operator is linear, and its spectral properties depend, in general, on the space of functions it acts upon [22–27]. It is a formal solution to the Liouville equation $\partial_t \rho + \nabla \cdot (\rho \mathbf{v}) = 0$, where $\dot{\mathbf{x}} = \mathbf{v}(\mathbf{x})$ is the dynamical system in examination. In chaotic Hamiltonian systems with no escape, the Perron-Frobenius spectrum has an isolated, unitary eigenvalue, whose ("leading") eigenfunction is uniform in the phase space, and it is called natural measure or invariant density [28]. The natural measure is the weight to every phase-space average, and, as such, its successful determination enables us to evaluate any long-term averaged observable under the ergodicity assumption, thus solving the problem of statistical mechanics. Here, instead, we focus on the other, "subleading" eigenfunctions of the Perron-Frobenius spectrum, whose eigenvalues yield the decay rate of any initial density to the natural measure. In a suitable functional space, we can expand the evolution of a density as

$$\mathcal{L}^t \rho(\mathbf{x}) = \sum_n a_n e^{-\gamma_n t} \phi_n(\mathbf{x}) + \sum_m a_m(t) \psi_m(\mathbf{x}), \tag{2}$$

where $\phi_0(\mathbf{x}) = 1$, $\gamma_0 = 0$, while the summation over n is an expansion over the eigenfunctions, all decaying with rates γ_n increasing with n, and the $\sum_m$ represents Jordan blocs, since the Perron-Frobenius operator is in general nondiagonalizable [its spectrum also has a continuous part, neglected in (2)]. In particular, $\phi_1(\mathbf{x})$ is hereafter referred to as second eigenfunction of the evolution operator.

In reality, every physical system experiences noise in some form, which is modeled as a random variable $\xi(t)$ in the equations of motion, $\dot{\mathbf{x}} = \mathbf{v}(\mathbf{x}) + \xi(t)$. If the noise is assumed as Gaussian-distributed and uncorrelated, the Liouville equation above acquires a diffusion term, say $D\nabla^2\rho$ (D is the noise amplitude or variance of ξ), and is known as Fokker-Planck equation. Its formal solution is a path ("Wiener") integral [29], whose kernel can be regarded as an evolution operator analogous to the Perron-Frobenius in Eq. (1), but with a finite-width

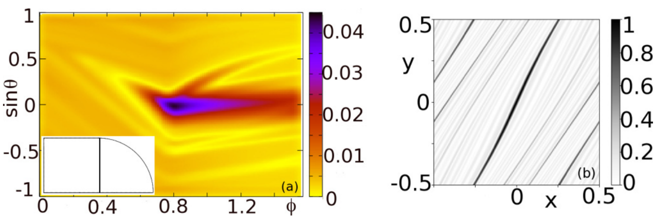

FIG. 1. Magnitude of the second eigenfunction of the noisy Perron-Frobenius operator, numerically evaluated for: (a) Bunimovich quarter stadium billiard (in the inset with the bouncing-ball orbit) with noise of amplitude $D = 10^{-2}$, using the Ulam matrix (3) with $N = 2^{14}$. Here $(\phi, \sin\theta)$ are the coordinates of the dynamics on the boundary of the billiard: ϕ is the polar angle locating the bounce, and $\sin\theta$ is the angle of incidence with the normal to the boundary; (b) perturbed cat map (periodic point at the origin) with $\epsilon = 0.1$, $\nu = 1$, using the scheme (4) with diffusivity $\Delta = 5 \times 10^{-3}$ and $M = 100$.

distribution instead of the delta function. Noise smears out densities, and thus it balances contractions from the deterministic, chaotic dynamics. Distributions of trajectories, as well as eigenfunctions of the noisy Perron-Frobenius operator, are then expected to be smooth.

Classical scars. Figure 1 illustrates localization of the subleading eigenfunctions of the noisy Perron-Frobenius operator near classical periodic orbits, for the Bunimovich quarter stadium billiard [30], as well as the cat map perturbed with a nonlinear shear, $(x', y') = (x + y - \frac{\varepsilon}{\nu}\sin(2\nu\pi y), x + 2y - \frac{\varepsilon}{\nu}\sin(2\nu\pi y)) \bmod 1$. In analogy with the corresponding enhancement of probability density of quantum eigenstates, we dub the observed phenomenon *classical scarring*, with the caveat that, to present knowledge, while some mechanisms behind the formation of scars are common in classical and in quantum mechanics, others may differ between the two. The dynamics of the cat map is everywhere unstable ("hyperbolic") [31], and the slowly-decaying eigenfunctions of the Perron-Frobenius spectrum are striated along the unstable manifold [32–35]. On the other hand, the stadium billiard is chaotic, ergodic [36], and has infinitely many unstable periodic orbits, but it also possesses a family of marginally stable ("bouncing ball") orbits that give rise to corresponding scars in the eigenfunctions of the quantized system [13,37,38]. An example of their classical counterpart is shown in Fig. 1(a). As for localization arising from unstable orbits in the stadium, results in Fig. 2 suggest that the same scars recur in distinct subleading eigenfunctions, and, conversely, that a single eigenfunction often displays several scars.

Methodology. The noisy Perron-Frobenius operator is projected onto a finite-dimensional vector space, and thus implemented as a finite matrix. Previous literature warns us that the choice of the discretization is crucial and may deeply affect the eigenspectrum beyond the leading eigenvalue in the linear map [39]. It has been established, on the other hand, that both nonlinear perturbations to linear maps on a torus, and background noise, increase the robustness of the numerically evaluated spectrum under certain conditions [23].

The simplest discretization scheme is Ulam's method [40], that amounts to subdividing the phase space into N intervals $\mathcal{M}_i$ of equal area. The evolution operator is thus approximated with a $N \times N$ transfer matrix whose entries $\mathbf{L}_{ij}$ are the transition probabilities from $\mathcal{M}_i$ to $\mathcal{M}_j$

$$\mathbf{L}_{ij} = \frac{\mu(\mathcal{M}_i \bigcap f_\xi(\mathcal{M}_j))}{\mu(\mathcal{M}_i)} \tag{3}$$

in one time step, where $f_\xi(\mathbf{x}) = f(\mathbf{x}) + \xi$ is the noisy mapping, while μ is the Lebesgue measure. We use a known Monte Carlo method [41] to estimate the nonsymmetric transfer matrix $\mathbf{L}_{ij}$, a (weighted) directed network [42], in today's parlance. A thorough study of stability and convergence of discretization algorithms has been reported elsewhere by the authors [43].

We implement Ulam's scheme for the Bunimovich quarter stadium, where more sophisticated discretizations (e.g., Markov partitions) appear impractical. On the other hand, the perturbed cat map also allows for an alternative realization of the transfer operator, by whose means we rule out the possibility that the detected scarring be just a numerical artifact. Since the dynamics of the cat map lives on the unit torus, a basis of smooth, periodic functions is suitable for the evolution operator, that can be defined in Fourier space as [44]

$$\mathcal{L}_\Delta \rho(\mathbf{x}) = \int \sum_{k_x,k_y}^{M} e^{2\pi i \mathbf{k}\cdot(f^{-1}(\mathbf{x})-\mathbf{x}_0)-\Delta \mathbf{k}^2} \rho(\mathbf{x}_0)\, d^2x_0. \tag{4}$$

Here the diffusivity Δ is equivalent to the variance D of the random variable ξ defined above in the Langevin picture. The spectrum of the operator in this basis is robust under perturbations [43] (e.g., dimension of the transfer matrix, noise amplitude, nonlinearity of the perturbed cat map), and classical scarring is consistently detected in the second eigenfunction of the spectrum: the one in Fig. 1(b) is computed with the Fourier basis of Eq. (4), while, for the same map, the

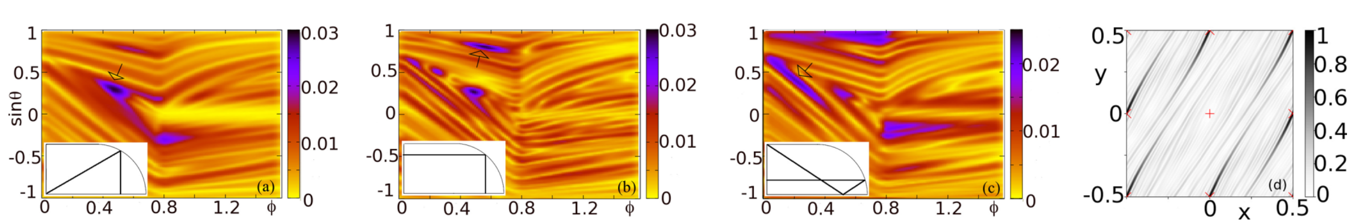

FIG. 2. Classical scars of short periodic orbits: (a)–(c) Bunimovich quarter stadium billiard. Here the Ulam matrix (3) has $N = 2^{14}$, and $D = 10^{-2}$. (a) Bowtie orbit (corresponding scar pointed to by an arrow); (b) rectangular orbit; (c) triangular orbit; (d) scar of a period-3 orbit [marked by $(\times)$] of the perturbed cat map ($\epsilon = 0.1$, $\nu = 2$) on the unit torus, obtained as the second eigenfunction of the transfer matrix (4), and $M = 50$, $\Delta = 10^{-5}$. The fixed point at the origin $(+)$ is "antiscarred".

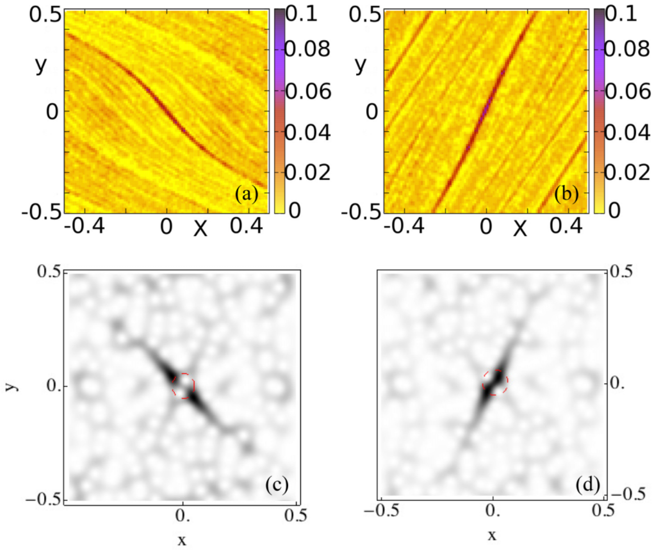

FIG. 3. The perturbed cat map: magnitudes of the (a) left- and (b) right-second eigenfunctions of the Perron-Frobenius operator, realized through the Ulam matrix (3), with $N = 10^4$, $D = 10^{-2}$; Husimi distributions of (c) right- and (d) left-eigenfunctions of the spectrum of the subunitary quantum propagator coupled to a single-channel opening (dashed circle). Details of the quantization in Ref. [46].

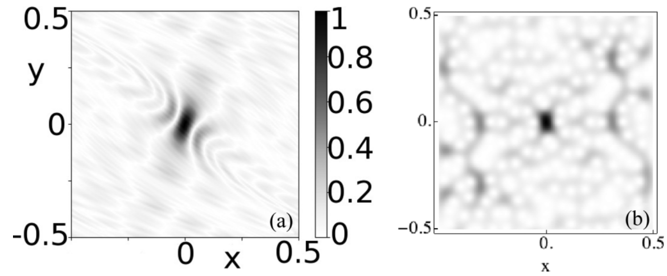

FIG. 4. (a) Unwrapping: the operator (6) is applied for $t = 3$ iterations to the second eigenfunction of the noisy Perron-Frobenius operator for the perturbed cat map [parameters as in Fig. 5(a)]; (b) Husimi distribution of a scarred eigenfunction of the unitary quantum propagator of the same map.

second eigenfunction of the Ulam matrix (3) is displayed in Fig. 3(b).

Analogy with quantum scars. The route to understand classical scarring begins by comparing it directly with its quantum counterpart. However, the propagator U^t, that regulates the evolution of quantum cat maps, is unitary [45], unlike our realizations of the noisy Perron-Frobenius operator $\mathcal{L}^t$, and that constitutes a clear asymmetry in our quest for classical-to-quantum correspondence. Breaking the unitarity of U^t by coupling the quantized cat map to an opening is the simplest way to restore the symmetry between classical and quantum evolution. The result is exemplified in Fig. 3, which features scars around the periodic orbit at the origin of the phase space, in both noisy classical and quantum cat maps. In the classical setting, the areas of enhanced probability density are striated along the stable- (left eigenfunction of $\mathcal{L}$) or unstable (right eigenfunction of $\mathcal{L}$) manifold, that emanates from the periodic orbit located at the origin. The correspondence left/right eigenfunction-stable/unstable manifold is less straightforward for the open quantum map [46], but still one-to-one.

Conversely, we may assimilate the classical scars to the original quantum scars of closed chaotic systems, where the propagation is unitary. Quantum scars of a unitary propagator are typically concentrated around a periodic orbit with no elongations on the manifolds, as a result of the unitary evolution. Using the known technique of eigenfunctions unwrapping [47], we map a right eigenfunction of the noisy $\mathcal{L}$ backward in time by means of the adjoint ("Koopman") evolution operator, whose noiseless definition reads

$$[\mathcal{L}^t]^\dagger \rho(\mathbf{x}) = \int dx_0\, \delta(\mathbf{x}_0 - f^t(\mathbf{x}))\rho(\mathbf{x}_0) = \rho(f^t(\mathbf{x})). \quad (5)$$

When noise is included and the Fourier representation (4) is used for $\mathcal{L}_\Delta$, the adjoint evolution operator is

$$\mathcal{L}_\Delta^\dagger \rho(\mathbf{x}) = \sum_{k_x,k_y}^{M} e^{2\pi i \mathbf{k}\cdot f(\mathbf{x}) - \Delta \mathbf{k}^2} \hat{\rho}_{\mathbf{k}}, \quad (6)$$

where the $\hat{\rho}_{\mathbf{k}}$'s are the Fourier coefficients of the density $\rho(\mathbf{x})$. Repeated adjoint mapping rids the eigenfunction of the striation along the unstable manifold, and regularizes it, until the outcome of Eq. (6) is almost invariant under both forward and backward iterations. The so-obtained unwrapped eigenfunction [Fig. 4(a)] now closely resembles its quantum analog [Fig. 4(b)].

Origin of classical scars. We now examine the local action of the classical Perron-Frobenius operator (1) on phase-space densities, in order to gain some insight on the mechanism behind classical scarring in uniformly hyperbolic systems such as the cat map:

$$\mathcal{L}^t \rho = \int dx_0\, \delta(\mathbf{x} - f^t(\mathbf{x}_0))\rho(\mathbf{x}_0) = \sum_{\mathbf{y}=f^{-t}(\mathbf{x})} \frac{\rho(\mathbf{y})}{|\det J^t(\mathbf{y})|}, \quad (7)$$

where $J^t_{ij}(\mathbf{y}) = \frac{\partial_i f^t(\mathbf{y})}{\partial y_j}$ is the Jacobian of the flow. Now restrict the analysis to the unstable manifold, where densities are stretched and squished. If the map is 2D, the unstable manifold is a locally 1D curve characterized by an arc length $s(\mathbf{y})$, and we indicate the restricted dynamics with $f_u(s)$, the corresponding evolution operator with $\mathcal{L}_u^t$, and a density on the manifold with $\rho_u(s)$. The mapping takes the form

$$\mathcal{L}_u^t \rho_u(s) \propto \prod_{k=0}^{t-1} \frac{1}{|[f_u^k(s)]'|} \rho_u(s) = e^{-\Lambda(\mathbf{y},t)t} \rho_u(s), \quad (8)$$

where $\Lambda(\mathbf{y}, t)$ is the finite-time Lyapunov exponent [48] of the map $f^t(\mathbf{x})$, that is the rate of exponential divergence of nearby trajectories within the time t. The last equality in Eq. (8) stems from the fact that the expanding rate of $f_u(s)$ is the stability multiplier of $f(\mathbf{x})$. On the other hand, assume that the relaxation of $\rho(\mathbf{y})$ towards equilibrium is well described by a truncation of the expansion (2), whose slowest-decaying term is almost entirely supported on the unstable manifold:

$$\mathcal{L}^t \rho(\mathbf{y}) \simeq a_0 + a_1 e^{-\gamma_1 t}\phi_1(\mathbf{y}) \sim a_0 + e^{-\Lambda(\mathbf{y},t)t} \rho_u(s). \quad (9)$$

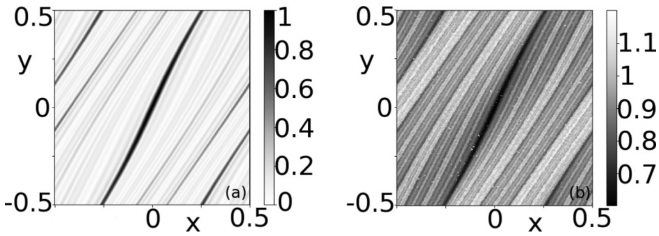

FIG. 5. (a) The second eigenfunction of the noisy Perron-Frobenius operator (4), numerically evaluated for a perturbed cat map with $\Delta = 10^{-2}$ and cutoff $M = 100$; (b) the phase-space distribution of the finite-time Lyapunov exponents ($t = 5$, sampling: 10^5 initial points) for the same map.

Since the evolution (8) of a density on the unstable manifold does not depend on the initial condition $\rho_u(s)$, we infer that $\Lambda(\mathbf{y}_1, t) > \Lambda(\mathbf{y}_2, t) \Rightarrow |\phi_1(\mathbf{y}_1)| < |\phi_1(\mathbf{y}_2)|$, and thus in general the probability density of the second eigenfunction of the spectrum along the unstable manifold is ruled by the finite-time Lyapunov exponent: the lesser instability, the higher the (magnitude of the) density [49–51]. As it can be inferred from Eq. (9), the Lyapunov exponent is to be evaluated over a time $t \simeq \gamma_1^{-1}$, thus of the order of the decay time of the eigenfunction $\phi_1(\mathbf{x})$. Densities stretch out along the unstable manifold, while they are contracted along the stable manifold. Asymptotically, the compression makes them infinitesimally thin, but noise counters that effect, and fattens densities along the unstable manifold. As a result, scarring also becomes apparent by visual inspection.

Figure 5 supports this hypothesis: The second eigenfunction of the noisy Perron-Frobenius operator is shown for the perturbed cat map, and it is localized along the unstable manifold that emanates from the origin. On the other hand, the numerically computed phase-space distribution of the finite-time Lyapunov exponent displays a suppression pattern that nearly overlaps with the scar.

Power spectra. Scarring can be quantified by studying the power spectrum [52]

$$S(\omega) = \frac{1}{\sqrt{T}} \sum_{t=0}^{T} \mathcal{C}(t) e^{2\pi i \omega t/T} \tag{10}$$

of a Gaussian density (the classical analog of a wave packet), that gradually decays into a uniform phase-space distribution, as the evolution operator is applied. Here $\mathcal{C}(t)$ is the autocorrelation function of the density [defined in Eq. (11)], while T is the length of the time series.

Figure 6 shows the outcome of the numerical experiment. A fast decay of $\mathcal{C}(t)$ occurs if we place the initial density at random in the phase space, resulting in a flat power spectrum. Instead, centering the initial distribution around the scarred fixed point [Fig. 6(a)] produces a slower decay in the autocorrelation function, and a peaked power spectrum. The quantum analog of $|S(\omega)|$ is the local density of states, whose energy-dependent, peaked envelope is a well-known signature of scarring [53]. The power spectrum is related to the second eigenfunction of the transfer operator in the following way. Truncating the expansion (2) at the first order, the autocorrelation function is estimated as

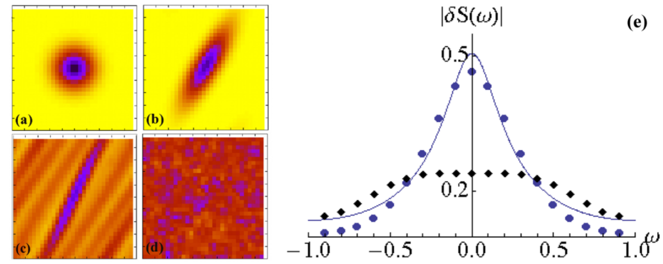

FIG. 6. (a) An initial Gaussian density centered at the fixed point of the perturbed cat map is mapped by the Ulam matrix (3); (b) t=1 iterations; (c) t=5; (d) t=20. (e) Magnitude of the power spectrum of the autocorrelation function minus the steady state: numerics for (dots) the density in (a)–(d), (diamonds) the same initial density centered at random in the phase space, (solid line) prediction (12).

$$\mathcal{C}(t) = \frac{\langle \rho_0, \mathcal{L}^t \rho_0 \rangle}{\langle \rho_0, \rho_0 \rangle} \approx c_0 + c_1 e^{-\gamma_1 t}, \tag{11}$$

for some c_0, c_1. Here $\langle \cdot, \cdot \rangle$ denotes the inner product. The discrete Fourier transform (10) of Eq. (11) then yields a delta function from the asymptotic overlap c_0 of the evolved density with the natural measure, plus the actual power spectrum of the exponential,

$$\delta S(\omega) \propto \frac{1}{1 - e^{i\omega T/2\pi - \gamma_1 t}}. \tag{12}$$

This approximation [solid line in Fig. (6)], with γ_1 determined from the diagonalization of the transfer matrix (3), shows close agreement with the direct numerical computation. Using the results of Eq. (9) and Fig. 5, one could replace γ_1 in Eq. (12) with the minimum finite-time Lyapunov exponent evaluated at $t \simeq \gamma_1^{-1}$.

Conclusion. We have reported the observation of classical scars, that is enhancement of probability density near periodic orbits, in the eigenfunctions of a noisy evolution operator of chaotic systems. We have detected scars in two model systems: perturbed cat maps, and the Bunimovich stadium billiard, both with background noise. For the cat map, the observed localization is ascribed to the inhomogeneity of instabilities near the periodic orbit of interest, on a time scale consistent with the decay rate of the second eigenfunction of the evolution operator, that is also the rate of correlation decay. In support of this argument, we have compared the second eigenfunction with the distribution of finite-time Lyapunov exponents of the dynamical system in exam. The inevitable presence of noise does not alter this mechanism, but merely thickens the scars by its smearing action along the unstable manifolds [cf. Figs. 1(b) and 5(a)]. Although we do not claim a one-to-one correspondence between classical and quantum scarring, we have pointed out apparent similarities in their phase-space patterns (provided the same symmetries) and power spectra, with the important difference of the time scales associated to the relevant instabilities. It is then natural to suppose that the mechanism at the origin of classical scars must also play a role in the formation of their quantum counterparts, in the same spirit as classical dynamical localization [54], or phase-space localization in open systems [3,55].

Acknowledgments. The authors are supported by NSF China (Grant No. 11750110416-1601190090) and JSPS KAKENHI (Grants No. 15H03701 and No. 17K05583). DL thanks S. Pascazio and R. Bellotti for hospitality at INFN Bari, and ReCaS Bari for computational resources.

[1] G. Casati, B. V. Chirikov, F. M. Izraelev, and J. Ford, in *Stochastic Behavior in Classical and Quantum Hamiltonian Systems*, edited by G. Casati and J. Ford, Lecture Notes in Physics Vol. 93 (Springer, Berlin, 1979).
[2] D. R. Grempel, S. Fishman, and R. E. Prange, Localization in an Incommensurate Potential: An Exactly Solvable Model, Phys. Rev. Lett. **49**, 833 (1982).
[3] K. Clauß, M. J. Körber, A. Bäcker, and R. Ketzmerick, Resonance Eigenfunction Hypothesis for Chaotic Systems, Phys. Rev. Lett. **121**, 074101 (2018).
[4] E. J. Heller, Bound-State Eigenfunctions of Classically Chaotic Hamiltonian Systems: Scars of Periodic Orbits, Phys. Rev. Lett. **53**, 1515 (1984).
[5] E. Bogomolny, Smoothed wave functions of chaotic quantum systems, Physica D **31**, 169 (1988).
[6] M. Srednicki, Chaos and quantum thermalization, Phys. Rev. E **50**, 888 (1994).
[7] C. J. Turner, A. A. Michailidis, D. A. Abanin, M. Serbyn, and Z. Papić, Weak ergodicity breaking from quantum many-body scars, Nat. Phys. **14**, 745 (2018).
[8] W. W. Ho, S. Choi, H. Pichler, and M. D. Lukin, Periodic Orbits, Entanglement, and Quantum Many-Body Scars in Constrained Models: Matrix Product State Approach, Phys. Rev. Lett. **122**, 040603 (2019).
[9] S. Choi, C. J. Turner, H. Pichler, W. W. Ho, A. A. Michailidis, Z. Papić, M. Serbyn, M. D. Lukin, and D. A. Abanin, Emergent SU(2) Dynamics and Perfect Quantum Many-Body Scars, Phys. Rev. Lett. **122**, 220603 (2019).
[10] C.-J. Lin and O. I. Motrunich, Exact Quantum Many-Body Scar States in the Rydberg-Blockaded Atom Chain, Phys. Rev. Lett. **122**, 173401 (2019).
[11] M. Schecter and T. Iadecola, Weak Ergodicity Breaking and Quantum Many-Body Scars in Spin-1 XY Magnets, Phys. Rev. Lett. **123**, 147201 (2019).
[12] S. Pai and M. Pretko, Dynamical Scar States in Driven Fracton Systems, Phys. Rev. Lett. **123**, 136401 (2019).
[13] E. Bogomolny and C. Schmit, Structure of Wave Functions of Pseudointegrable Billiards, Phys. Rev. Lett. **92**, 244102 (2004).
[14] M. Lebental, N. Djellali, C. Arnaud, J.-S. Lauret, J. Zyss, R. Dubertrand, C. Schmit, and E. Bogomolny, Inferring periodic orbits from spectra of simply shaped microlasers, Phys. Rev. A **76**, 023830 (2007).
[15] B. Dietz, T. Friedrich, M. Miski-Oglu, A. Richter, and F. Schäfer, Properties of nodal domains in a pseudointegrable barrier billiard, Phys. Rev. E **78**, 045201(R) (2008).
[16] P. J. J. Luukko, B. Drury, A. Klales, L. Kaplan, E. J. Heller, and E. Räsänen, Strong quantum scars by local impurities, Sci. Rep. **6**, 37656 (2016).
[17] J. Keski-Rahkonen, P. J. J. Luukko, L. Kaplan, E. J. Heller, E. Räsänen, Controllable quantum scars in semiconductor quantum dots, Phys. Rev. B **96**, 094204 (2017).
[18] J. Keski-Rahkonen, A. Ruhanen, E. J. Heller, E. Räsänen, Quantum Lissajous Scars, Phys. Rev. Lett. **123**, 214101 (2019).
[19] L. Huang, Y.-C. Lai, D. K. Ferry, S. M. Goodnick, and R. Akis, Relativistic Quantum Scars, Phys. Rev. Lett. **103**, 054101 (2009).
[20] M.-Y. Song, Z.-Y. Li, H.-Y. Xu, L. Huang, and Y.-C. Lai, Quantization of massive Dirac billiards and unification of nonrelativistic and relativistic chiral quantum scars, Phys. Rev. Research **1**, 033008 (2019).
[21] P. Cvitanović, R. Artuso, R. Mainieri, G. Tanner, and G. Vattay, *Chaos: Classical and Quantum*, `ChaosBook.org` (Niels Bohr Institute, Copenhagen, 2016)
[22] D. Dolgopyat, On decay of correlations in Anosov flows, Ann. Math. **147**, 357 (1998).
[23] M. Blank, G. Keller, and C. Liverani, Ruelle-Perron-Frobenius spectrum for Anosov maps, Nonlinearity **15**, 1905 (2002).
[24] C. Liverani, On contact Anosov flows, Ann. Math. **159**, 1275 (2004).
[25] R. Markarian, Billiards with polynomial decay of correlations, Ergod. Th. Dynam. Sys. **24**, 177 (2004).
[26] H. H. Rugh, The correlation spectrum for hyperbolic analytic maps, Nonlinearity **5**, 1237 (1992).
[27] J. D. Crawford and J. R. Cary, Decay of correlations in a chaotic measure-preserving transformation, Physica D **6**, 223 (1983).
[28] P. Gaspard, *Chaos, Scattering, and Statistical Mechanics* (Cambridge University Press, Cambridge, 1999)
[29] H. Risken, *The Fokker-Planck Equation* (Springer, Berlin, 1996)
[30] L. A. Bunimovich, Funct. Anal. Appl. **8**, 254 (1974).
[31] V. I. Arnold and A. Avez, *Ergodic Problems of Classical Mechanics*, (Benjamin, New York, 1968)
[32] J. Weber, F. Haake, and P. Seba, Frobenius-Perron Resonances for Maps with a Mixed Phase Space, Phys. Rev. Lett. **85**, 3620 (2000).
[33] G. Blum and O. Agam, Leading Ruelle resonances of chaotic maps, Phys. Rev. E **62**, 1977 (2000).
[34] J. Weber, F. Haake, P. A. Braun, C. Manderfeld and P. Seba, Resonances of the Frobenius-Perron operator for a Hamiltonian map with a mixed phase space, J. Phys. A **34**, 7195 (2001).
[35] C. Manderfeld, Classical resonances and quantum scarring, J. Phys. A **36**, 6379 (2003).
[36] L. A. Bunimovich, On the ergodic properties of nowhere dispersing billiards, Commun. Math. Phys. **65**, 295 (1979).
[37] A. Hassell, Ergodic billiards that are not quantum unique ergodic, Ann. Math. **171**, 605 (2010).
[38] M. Sieber, U. Smilanksy, S. C. Creagh, and R. G. Littlejohn, Non-generic spectral statistics in the quantized stadium billiard, J. Phys. A **26**, 6217 (1993).
[39] F. Brini, S. Siboni, G. Turchetti, and S. Vaienti, Decay of correlations for the automorphism of the torus $\mathbb{T}^2$, Nonlinearity **10**, 1257 (1997).
[40] S. M. Ulam, *A Collection of Mathematical Problems* (Interscience, New York, 1960).

[41] L. Ermann and D. L. Shepelyansky, The Arnold cat map, the Ulam method, and time reversal, Physica D **241**, 514 (2012).

[42] A.-L. Barabási, *Network Science* (Cambridge University Press, Cambridge, 2016).

[43] K. Yoshida, H. Yoshino, A. Shudo, and D. Lippolis, Eigenfunctions of the Perron-Frobenius operator and the finite-time Lyapunov exponents in uniformly hyperbolic area-preserving maps, arXiv:2101.11701.

[44] J. L. Thiffeault and S. Childress, Chaotic mixing in a torus map, Chaos **13**, 502 (2003).

[45] S. C. Creagh, Quantum zeta function for perturbed cat maps, Chaos **5**, 477 (1995).

[46] D. Lippolis, J. W. Ryu, S. Y. Lee, and S. W. Kim, On-manifold localization in open quantum maps, Phys. Rev E **86**, 066213 (2012).

[47] G. Froyland, Unwrapping eigenfunctions to discover the geometry of almost-invariant sets in hyperbolic maps, Physica D **237**, 840 (2008).

[48] H. Fujisaka, Statistical Dynamics Generated by Fluctuations of Local Lyapunov Exponents, Prog. Theor. Phys. **70**, 1264 (1983).

[49] P. H. Haynes and J. Vanneste, What controls the decay of passive scalars in smooth flows? Phys. Fluids **17**, 097103 (2005).

[50] J.-L. Thiffeault, Scalar decay in chaotic mixing, Lect. Notes Phys. **744**, 3 (2008).

[51] G. Haller, Lagrangian coherent structures, Annu. Rev. Fluid Mech. **47**, 137 (2015).

[52] T. M. Antonsen, Z. Fan, E. Ott, and E. Garcia-Lopez, The role of chaotic orbits in the determination of power spectra of passive scalars, Phys. Fluids **8**, 3094 (1996).

[53] L. Kaplan and E. J. Heller, Linear and nonlinear theory of eigenfunction scars, Ann. Phys. (NY) **264**, 171 (1998).

[54] I. Guarneri, G. Casati, and V. Karle, Classical Dynamical Localization, Phys. Rev. Lett. **113**, 174101 (2014).

[55] K. Clauß, E. G. Altmann, A. Bäcker, and R. Ketzmerick, Structure of resonance eigenfunctions for chaotic systems with partial escape, Phys. Rev. E **100**, 052205 (2019).